



# BRNO UNIVERSITY OF TECHNOLOGY

VYSOKÉ UČENÍ TECHNICKÉ V BRNĚ

## FACULTY OF ELECTRICAL ENGINEERING AND COMMUNICATION

FAKULTA ELEKTROTECHNIKY  
A KOMUNIKAČNÍCH TECHNOLOGIÍ

## DEPARTMENT OF RADIO ELECTRONICS

ÚSTAV RADIOELEKTRONIKY

## 3D PRINTED ARTIFICIAL MATERIALS FOR MICROWAVE STRUCTURES

3D TIŠTĚNÉ UMĚLÉ MATERIÁLY PRO MIKROVLNNÉ STRUKTURY

### SHORT VERSION OF DOCTORAL THESIS

TEZE DIZERTAČNÍ PRÁCE

#### AUTHOR

AUTOR PRÁCE

Ing. Petr Kaděra

#### SUPERVISOR

ŠKOLITEL

doc. Ing. Jaroslav Láčák, Ph.D.

BRNO 2022

## **Keywords**

3D printing, artificial dielectrics, artificial materials, dielectric substrate, parallel plate capacitor, effective medium theory, additive manufacturing, lens antenna, material characterization, millimeter-waves, spatial permittivity distribution, retroreflector.

## **Klíčová slova**

3D tisk, umělá dielektrika, umělé materiály, dielektrické substráty, kapacitory s paralelními elektrodami, teorie efektivního média, aditivní výroba, čočková anténa, charakterizace materiálu, milimetrové vlny, prostorová distribuce permittivity, retroreflektor.

## **Storage place**

Research department, FEEC BUT, Technická 3058/10, 602 00 Brno

## **Místo uložení práce**

Vědecké oddělení, FEKT VUT v Brně, Technická 3058/10, 602 00 Brno

© Petr Kaděra, 2022

ISBN (80-214-)

ISSN 1213-4198

# Contents

<b>1</b>	<b>Introduction</b>	<b>5</b>
<b>2</b>	<b>State-of-the-Art</b>	<b>6</b>
2.1	3D Printed Artificial Substrates.....	6
2.1.1	Effective Medium Theory Approximations .....	7
2.1.2	Electrical Network Methods .....	8
2.1.3	Multi-Modal Transfer Matrix Method .....	9
2.1.4	Numerical Methods.....	10
2.1.5	Materials and Tunability of Their properties .....	11
2.2	3D Printed and Spatial Permittivity Distributed Lens Antennas .....	12
2.2.1	Lenses with Spatial Permittivity Distribution .....	12
2.2.2	Retroreflecting Lenses .....	12
<b>3</b>	<b>Objectives of Thesis</b>	<b>14</b>
<b>4</b>	<b>State-of-the-Work</b>	<b>15</b>
4.1	Objective 1 .....	15
4.2	Objective 2 .....	16
4.3	Objective 3 .....	17
<b>5</b>	<b>Conclusions and Future Work</b>	<b>21</b>
	<b>Bibliography</b>	<b>23</b>
	<b>Selected Publications of the Author</b>	<b>27</b>
	<b>Other Publications of the Author</b>	<b>27</b>
	<b>Curriculum Vitae</b>	<b>28</b>
	<b>Abstract</b>	<b>30</b>



# 1 Introduction

Improvements in additive manufacturing technology during recent years have enabled three-dimensional (3D) printing technology to be used for fast prototype design and complex shape construction that are hardly manufacturable by conventional subtractive methods such as computer numeric control (CNC) machining or chemical etching. 3D printing also allows an extra degree of freedom in the tunability of the electromagnetic (EM) properties of the structures, complemented by less waste of used material, or general decrease of manufacturing costs, especially for prototyping and low-quantity fabrication [1].

3D printing technologies can be used for developing periodic structures with engineered EM properties, for example, artificial dielectric substrates with spatial permittivity distribution allowing to attain an equivalent permittivity range as composition of several conventional dielectric substrates with different permittivity values. The benefit of such artificially engineered dielectric substrates lies in their fabrication, since they can be monolithically 3D printed from a single material. For a practical design, it is mandatory to know the exact values of the given EM properties, and any inaccuracy leads to often intolerable disagreements between the desired and achieved performance. The conventional approach used for characterization of such structures is an implementation of the effective medium theory approximations (EMAs) that mainly considers an inclusion to a host material volume ratio, further referred to as inclusion volume fraction, with limited consideration of the implied EM wave polarization effect [2].

To provide more accurate predictions, the effective constitutive parameters such as the effective permittivity and effective permeability of differently shaped artificial substrate unit cells with a predefined spatial distribution have to be described in a different way. The parallel plate capacitor (PPC) networks approach [3], which can consider a real physical shape of the structure, appears promising for further investigation and development of the models describing effective constitutive parameters of dielectric structures. However, simultaneous description of both the effective permittivity and effective permeability of artificial substrates containing metallic and dielectric inclusions is an ambiguous task that requires knowledge of the effective impedance of the medium. Due to this reason, an effective approach to determining the EM properties of the artificial substrates is found in the multi-modal transfer matrix method (MMTMM) [4], which enables the retrieval of constitutive parameters in the volumetric space of the entire unit cell what is suitable for 3D printed structures.

Within the framework of artificial substrates that possess spatially distributed EM properties, gradient-index (GRIN) based lenses offer a prospective space for further performance improvements in the area of passive, chipless frequency-coded millimeter-wave retroreflectors [5]. Increasing the maximum detection range, achieving a wide angular coverage, stable radar cross section (RCS) response, and monolithic integrations of frequency-coded retroreflector designs are highly desired. Since the frequency-coded retroreflectors may serve as anchors in the space, e.g. being built inside walls, they can find an application in an indoor environment for self-localization of the devices, e.g. drones, when there is no availability of the global positioning system (GPS). Further, the accuracy of a device's localization and ranging is influenced by the maximum achievable absolute bandwidth of a radar system. Thus, moving from centimeter waves to millimeter waves and even higher towards sub-THz and THz frequencies is demanding for larger frequency bandwidths, i.e. fine time resolution required for high spatial detection accuracy [6]. Therefore, lenses with spatially variant permittivity profiles and their possible wide angular coverage and stable RCS enhancement of frequency-coded retroreflectors are another point of interest in the following chapters of this thesis.

## 2 State-of-the-Art

An introduction into the 3D printed artificial periodic structures and dielectric substrates as the building elements exploitable for antenna and microwave designs is presented in this chapter. Basic limitations and advantages of conventional and intended design approaches are discussed. The electromagnetic properties of materials used in 3D printing are compared with those of common commercially available materials, and attention is turned to lenses with spatial distribution of the effective permittivity for wide angular coverage and stable RCS enhancements of passive, chipless frequency-coded millimeter-wave retroreflectors.

### 2.1 3D Printed Artificial Substrates

The 3D printed artificial substrates can be considered as a subset of artificial dielectrics with controlled effective permittivity/permeability values which can be regulated by the inclusions volume fraction, i.e. the ratio between the inclusions of some material embedded in another, a host material [7]. Typical examples of these structures are perforated dielectrics [8], grounded cuboidal metallic posts [9], or inclusions of various shapes in a two-dimensional or three-dimensional periodic lattice of the host medium [10]-[12]. Furthermore, the effective EM parameters of artificial substrates are frequently obtained directly by measurements without prior predictive analysis that estimates their tunability range of the EM parameters and anisotropic behavior [13].

In principle, 3D printed artificial dielectric substrates are created by adding top and bottom covering layers on the base inclusions pattern, which is filled by a chosen material. The covering layers then introduce some degree of structure's anisotropy and their effects are more discussed in [12]. Note that in this thesis, we dominantly focus on the EM parameters in the parallel and perpendicular polarization directions, as they represent the boundaries between which the EM parameters can take values even for oblique EM wave incidence.

The importance of accurate knowledge of the effective permittivity and effective permeability tensor values is obvious in phase sensitive antenna and microwave design applications. For example, phase shifters for feeding antenna arrays [14], long microstrip transmission lines and microwave filters [15], or circularly polarized antennas [16]. Improvement in predictive models can, therefore, make the designs more efficient.

The typical inclusions patterns of the artificial dielectric substrates are depicted in Fig. 2.1. The inclusions are colored in cyan, and the host is colored in yellow.

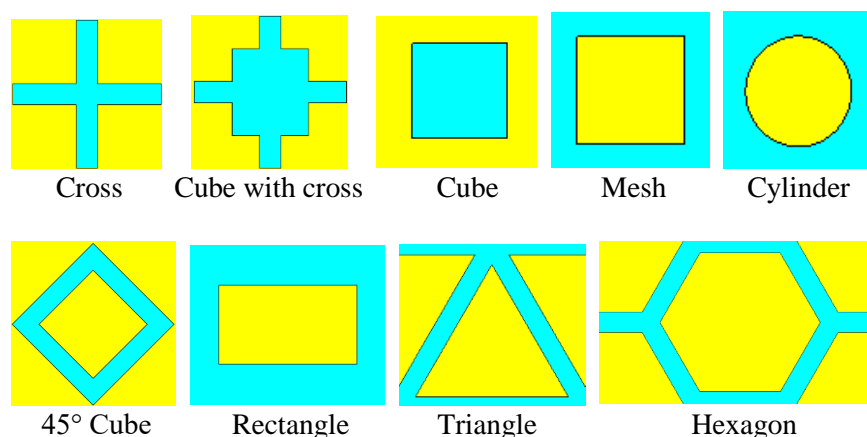


Fig. 2.1 Typical inner inclusions patterns of artificial dielectric substrates.

### 2.1.1 Effective Medium Theory Approximations

The purpose of the effective medium theory (EMT) concept is to characterize the dielectric properties of heterogeneous mixtures containing microscopic particles with a defined inclusions volume fraction. Effective in these terms means that the composite mixture responds to electromagnetic excitation as it would be homogeneous. The main limitation of the EMT is the impossibility to predict resonance behavior of the studied structures, so the general requirement on the inclusions size is that they have to be sub-wavelength, typically smaller than  $\lambda_0/10$ . However, this restriction is related to the assumption that subwavelength structures can be analyzed from a quasi-static point of view [17]. On the other hand, the advantage of EMT is its applicability to magnetic, magnetoelectric, and to some extent, even to anisotropic materials [2].

The summary of various effective medium approximations (EMA) used for determination of the effective permittivity is presented in [2]. The best known EMA is the Maxwell Garnett (MG) mixing formula (Eq. 2.1). In general, the formula is suitable for isotropic inclusions such as cubes or spheres.

$$\varepsilon_{\text{eff}} = \varepsilon_h + 3f\varepsilon_h \frac{\varepsilon_i - \varepsilon_h}{\varepsilon_i + 2\varepsilon_h - f(\varepsilon_i - \varepsilon_h)}, \quad (2.1)$$

where  $\varepsilon_{\text{eff}}$  denotes the effective permittivity,  $f$  is the inclusions volume fraction,  $\varepsilon_h$  represents the permittivity of the host medium and  $\varepsilon_i$  is the permittivity of the inclusions.

Although the MG EMA formula is commonly employed, its drawback might be in non-symmetry which may limit its applicability in the situation when the inclusions volume fraction is comparable to or higher than the host medium. For that case, another important EMA formula, the symmetric Bruggeman formula defined by Eq. (2.2) may provide more accurate results [18].

$$\frac{\varepsilon_{\text{eff}} - \varepsilon_h}{\varepsilon_{\text{eff}} + 2\varepsilon_h} = \sum_{n=1}^N f_n \frac{\varepsilon_n - \varepsilon_h}{\varepsilon_n + 2\varepsilon_h} \quad (2.2)$$

For mixtures with random geometry that could not be accurately described by the MG or Bruggeman EMAs, several alternative and more generalized formulas might be potentially more successful. In particular, the power-law (Lichtenecker) approximations given by Eq. (2.3), with variable parameter  $a$  (for  $a = 1/2$ , named as the Birchak formula, for  $a = 1/3$ , named as the Looyenga formula, or for  $a = 1$ , represents the linear law) are widely known.

$$\varepsilon_{\text{eff}}^a = f\varepsilon_i^a + (1-f)\varepsilon_h^a \quad (2.3)$$

Another important issue connected with the effective permittivity prediction is the question of boundaries within which the permittivity values can lie. Widely spread is a Wiener limit defined by maximum (Eq. 2.4) and minimum (Eq. 2.5) bounds [18]. These boundaries define the extreme values of the effective permittivity which the studied effective medium exhibits in a non-resonant state for the given inclusion volume fraction.

$$\varepsilon_{\text{eff}}^{\text{max}} = f\varepsilon_i + (1-f)\varepsilon_h \quad (2.4)$$

$$\varepsilon_{\text{eff}}^{\text{min}} = \frac{\varepsilon_i\varepsilon_h}{f\varepsilon_h + (1-f)\varepsilon_i} \quad (2.5)$$

The less strict boundaries for isotropic mixtures can be determined by upper and lower Hashin-Shtrikman (HS) bounds, which can provide satisfactory results in the case of honeycomb and pyramidal structures [19]. The study in [20] then states that the selected inclusions patterns can be described by the previously mentioned EMAs, but for more complex shapes, none of them can generally be used. The example of selected 2D inclusions distribution patterns with various EMA formulas and their results is shown in Fig. 2.3.

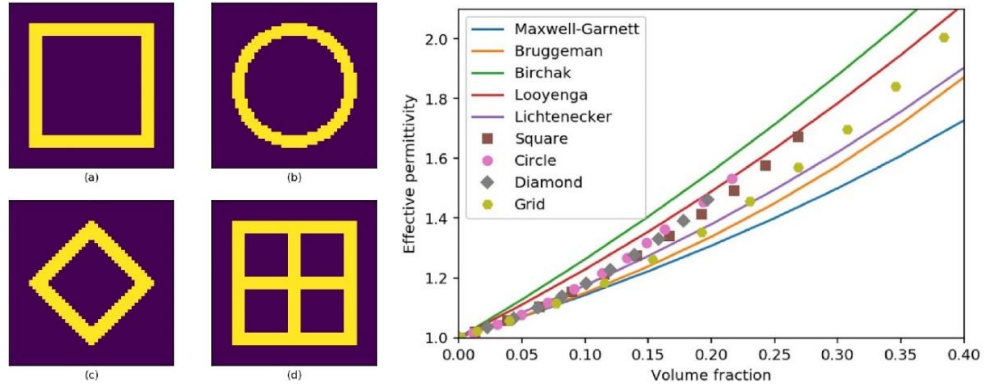


Fig. 2.3 Patterns of hollow inclusions ((a) square, (b) circle, (c) diamond, (d) grid) – left, effective permittivity of different inclusions shapes in two dimensions, the permittivity of inclusions (yellow) and host medium (purple) are 5 and 1, respectively – right from [20] with permission © 2019 from Elsevier.

The problem is further complicated in the case of conductive inclusions, where for example, the MG and Bruggeman EMA formulas can be exploited for the effective conductivity calculations of lattices with  $45^\circ$  rotated cubes [21]. Similarly, as in the effective permittivity calculation, the effective permeability of the mixture can be evaluated using the same formula (Eq. 2.1) by replacing permittivity with permeability [22]. The exploitation of 3D printed conductive inclusions in a dielectric host medium is typically found not only in the field of artificial substrates but also in antenna miniaturization [23], or microwave components such as artificially engineered high-frequency capacitors [24].

## 2.1.2 Electrical Network Methods

A potential analytical approach for the determination of the effective permittivity of dielectric structures that could overcome the shortcomings mentioned in the previous chapters lies in exploiting the parallel plate capacitor (PPC) networks method presented in [3]. This method is based on the division of a real dielectric structure into individual sub-cells which create parallel plate capacitors that are mutually connected in the electric network arrangement depending on the discretization of the structure. The effective permittivity is then calculated from the equivalent capacitance of this network and the known dimensions of the analyzed structure. The advantage of this method is that it allows describing more complexly shaped structures with a predefined geometry, their subsequent parameterization and faster computation than the finite element method (FEM), when the discretization is done numerically [25]. Since 3D printed artificial dielectric substrates belong to this kind of structures, the PPC method will be further investigated and compared with the conventional EMAs, including the accuracy evaluation. However, it is important to pay increased attention to the proper selection of discretization scheme for effective permittivity calculations [11]. An example of such a structure involving vertical and horizontal discretization is demonstrated in Fig. 2.4.

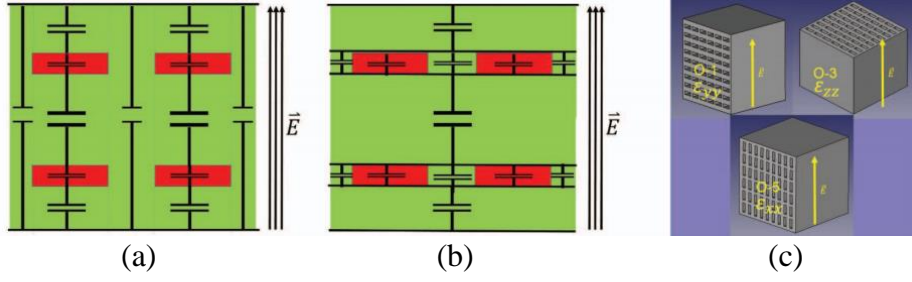


Fig. 2.4 Capacitors in vertical discretization (a), capacitors in horizontal discretization (b), cubical sample with rectangular inclusions (c) from [11] with permission © 2015 IEEE.

In general, the PPC method assumes only capacitive and resistive elements (RC) [3], which limit the use of this method to the dielectric only inclusions including their dielectric losses. Such structures are described by the complex effective permittivity which can be approximated by frequency-dependent dielectric relaxation models (e.g. Debye, Cole-Cole) [26], or by the initial wide-band measurements of the EM properties of the materials. If we want to include conductive inclusions in the predictive model, we need to derive equivalent circuit networks involving simple lumped element (RLC), which may not involve dispersion behavior of the structures [27], or find a suitable topology and components that account for the incident wave scattering and higher order modes coupling, including transmission lines and spatially distributed impedances, or admittances, what can be complicated [28].

### 2.1.3 Multi-Modal Transfer Matrix Method

A promising approach to the problem related to the effective constitutive parameters determination is found in the exploitation of a hybrid multi-modal transfer matrix method (MMTMM) [29]-[30]. The MMTMM is based on a combination of numerical and analytical approaches. In the first step, an initial numerical simulation is performed over the targeted frequency range to obtain the scattering parameters of the structure studied. In the second step, the scattering matrix is transformed into a multimodal transfer matrix (ABCD), which relates the voltages and currents on the input and output ports, as is demonstrated in Fig. 2.5. From the Bloch's theorem [31], one can relate the phase shift across the given unit cell and its periodicity to the ABCD matrix and by solving the frequency-dependent eigenproblem, eigenvalues and eigenvectors needed for retrieval of constitutive effective parameters are calculated. The advantage of the MMTMM is that it provides the complex dispersive behavior of the structure, including losses in both the passband and stopband frequency ranges. When the MMTMM is used with multiple ports, even 3D periodic structures can be analyzed [32].

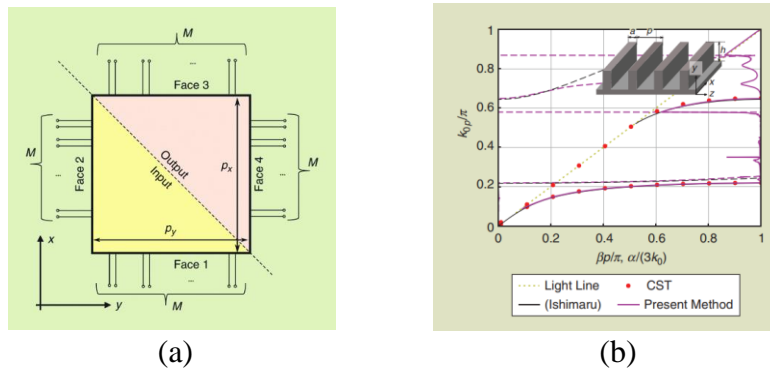


Fig. 2.5 Principal schematic of the multimodal transfer matrix method used for 2D periodic structure (a), dispersion diagram of 1D corrugated PEC surface (b) from [30] with permission © 2021 IEEE.

Up to recently, periodic EM structures analyzed by the MMTMM have been defined by a square shape that represented the smallest possible unit cell. However, when the analyzed structures create a rectangular unit cell, e.g. hexagons, they do not represent the smallest possible unit cell, but rather a larger structure, i.e. a supercell. This leads to multiple eigenproblem solutions outside the first Brillouin zone that manifest themselves as modes folding into the first Brillouin zone, as shown in Fig. 2.6. A recent study on this phenomenon in periodic EM structures was published in [33], and further development of the MMTMM is required to include this effect, e.g. by employing modes unfolding algorithms [34].

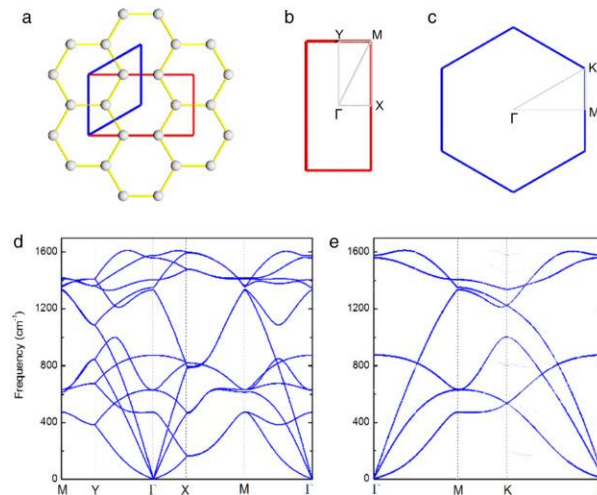


Fig. 2.6 Atomic structure of graphene with its supercell (red rectangle) and primary cell (blue parallelogram) (a). Panels (b) and (c) show the first Brillouin zones of the supercell and the primary cell, respectively, with high symmetry points and lines. Panel (d) shows the phonon dispersions of the supercell. Panel (e) shows the phonon dispersions unfolded into the primary-cell Brillouin zone from [34] with permission © 2016 from Elsevier.

## 2.1.4 Numerical Methods

In the field of numerical simulations, the effective permittivity can be extracted by several methods. The extraction of EM parameters based on a dispersion diagram is an easily applicable numerical method [35]. For its calculation, the eigenmode solver in commercial computer aided design (CAD) electromagnetics software can be used. The effective relative permittivity  $\varepsilon_{r,\text{eff}}$  is then extracted by Eqs. (2.6) and (2.7).

$$\varepsilon_{r,\text{eff}} = \left( \frac{\beta \lambda_0}{2\pi} \right)^2, \quad (2.6)$$

where  $\beta$  denotes the propagation constant and  $\lambda_0$  is the free-space wavelength.

$$\beta = \frac{\Delta\varphi}{l}, \quad (2.7)$$

where  $\Delta\varphi$  represents the phase difference and  $l$  is the length over which the phase change applies (or periodicity).

However, the disadvantage of the eigenmode approach implemented in the commercial numerical solvers lies in inability to calculate the complex dispersion diagrams, i.e. the imaginary part of the complex propagation constant representing the attenuation constant.

Another method exploitable for the effective permittivity and effective permeability extraction is the transmission/reflection method based on the Nicholson-Ross-Weir (NRW) algorithm, which uses the transmission ( $S_{21}$ ) and reflection ( $S_{11}$ ) coefficients obtained from the scattering parameters at the input and output ports of a waveguide or a coaxial line [36]. For practical measurement, its improved iterative version, which does not require the sample to touch at the reference planes, should be used [37]. Similarly, the free-space or transmission line methods can be exploited [38]. All these techniques are generally broadband, but their precision for  $\tan(\delta)$  determination is often limited, up to the range of  $10^{-2}$ - $10^{-3}$ .

Another method which is suitable for the extraction of the material's effective EM properties of low-loss materials with  $\tan(\delta)$  down to  $10^{-6}$  is based on the perturbation theory and uses both narrowband resonators and wideband split-post dielectric resonators (SPDR) [39]. In principle, the effective relative permittivity is determined by the frequency shift between the unloaded and sample loaded resonator states, and the dielectric losses depend on the corresponding Q-factors.

### 2.1.5 Materials and Tunability of Their Properties

The materials used in 3D printing technology are being continuously developed as the demands on their desired properties are still increasing. The range in which the EM properties can be tuned is limited mainly due to their relative permittivity, relative permeability, and associated dielectric losses/conductivity of the materials at a given frequency range.

Common materials used in fused decomposition modeling (FDM) 3D printing comprise polylactic acid (PLA), acrylonitrile butadiene styrene (ABS), polyethylene terephthalate (PET), polycarbonate (PC), high-density polyethylene (HDPE), nylon, high-impact polystyrene (HIPS), and mixtures with carbon fibers, cork, wood, steel, copper, or ceramics. The materials used for conventional stereolithography (SLA), two-photon polymerization (TPP), and polymer-jetting (PJ) 3D printing are mostly UV curable resins, and for ceramic SLA, the special oxides such as alumina ( $\text{Al}_2\text{O}_3$ ) or zirconia ( $\text{ZrO}_2$ ) are possible to be used. Compared to additive 3D printing techniques, conventional subtractive methods use materials such as Rexolite, Teflon, Rogers<sup>®</sup> dielectric substrates, or high-resistive silicon (HR-Si). Moreover, even materials with high conductivity such as the Electrifi filament or special conductive pastes are of great interest in the electrical engineering field. The summarization of the EM properties (permittivity  $\epsilon_r$ , dielectric loss  $\tan(\delta)$ , electrical conductivity  $\sigma$ ) of the selected materials is presented in Table 2.1.

Table 2.1 Electromagnetic properties of selected materials used in additive (3DP) and subtractive technology.

Material	Parameters @ frequency	Technology	Ref.
PLA	$\epsilon_r = 2.71$ , $\tan(\delta) = 0.0063$ @ 10 GHz	FDM 3DP	[40]
ABS	$\epsilon_r = 2.6$ , $\tan(\delta) = 0.0054$ @ 10 GHz	FDM 3DP	[40]
PC	$\epsilon_r = 2.68$ , $\tan(\delta) = 0.002$ @ 100 GHz	FDM 3DP	[41]
Alumina	$\epsilon_r = 9.5$ , $\tan(\delta) = 0.0004$ @ 100 GHz	SLA 3DP Subtractive	[42]
Rogers <sup>®</sup> RT Duroid 6010	$\epsilon_r = 10.2$ , $\tan(\delta) = 0.0023$ @ 10 GHz	Subtractive	[43]
HiRe-Silicon	$\epsilon_r = 11.68$ , $\tan(\delta) = 0.00015$ @ 100 GHz	Subtractive	[42]
DuPont CB028 ink	$\sigma_{DC} = 4.76 \cdot 10^6$ S/m / $\sigma = 2 \cdot 10^5$ S/m @ 10 GHz	FDM 3DP	[44]

## 2.2 3D Printed and Spatial Permittivity Distributed Lens Antennas

The most promising applications of structures with a spatial permittivity distribution can be found in the engineering field of gradient permittivity lenses, lens antennas, and microwave filters.

### 2.2.1 Lenses with Spatial Permittivity Distribution

The lenses and structures with spatial distribution of EM properties can be employed in many applications. For example, they can be used for aperture phase correction of horn antennas [45], excitation of hybrid modes in dielectric loaded antennas to enhance antenna gain and aperture efficiency [46], beamforming applications for radar imaging and multiple-input-multiple-output (MIMO) communications [47], or enabling an ultra-wideband performance [48]. Spatially distributed inclusions of artificial dielectric substrates can be exploited to broaden the impedance bandwidth of patch antennas [49], or to enable the generation of a circularly polarized wave by a linearly polarized dipole antenna [50].

A very promising technique is the quasi-conformal transformation optics (QCTO), which is applicable for transforming the radiation pattern of patch antennas, e.g. to behave like a dipole antenna, to enlarge the half-power beam-width (HPBW) from  $90^\circ$  to  $300^\circ$ , or to shift the main lobe from the elevation direction to the azimuthal direction [51]. The advantage of the QCTO over the traditional transformation optics (TO) methods is that the calculated spatial distribution of the effective EM parameters allows the exploitation of isotropic or uniaxially anisotropic dielectric materials, which are better accessible in various fabrication methods than biaxially anisotropic and magnetic materials [52]. The QCTO technique enables to transform the geometry of a structure into a new desired shape with a good preservation of its original performance, for example, a liquid-based QCTO Luneburg lens with an ultra-wide-angle beam steering capability of  $\pm 90^\circ$  was demonstrated in [53]. With these regards, the QCTO has a large potential to be easily implemented for applications requiring wide-angle beam-scanning antenna performance.

However, a common problem with the combination of QCTO lenses and planar antenna array feeds is their poor impedance matching. This issue was first addressed in [54], by adding an anti-reflective layer that helped to maintain a stable antenna gain of a QCTO Luneburg lens in the angular range of  $\pm 55^\circ$ . Nevertheless, further studies on this effect for higher beam scanning angles and higher relative permittivities that ceramic materials can achieve are still missing.

### 2.2.2 Retroreflecting Lenses

Another area where the QCTO-based structures have a large potential of performance enhancements are retroreflectors. Retroreflectors are structures that retransmit an EM wave in its incidental direction. In [55], a metallic trihedral corner reflector was replaced by a dielectric compressed reflector. Similarly, a parabolic reflector with the main beam reflected in a single direction up to  $\pm 47^\circ$  away from the broadside was realized in [56]. Further, as a retroreflector can be exploited a Luneburg lens backed by a slant polarizer to enable omnidirectional reflections [57].

The combination of lenses with spatially distributed permittivity, especially when combined with the QCTO technique, is potentially very promising for frequency-coded passive, chipless retroreflectors enabling high-accuracy RFID for an indoor localization in

millimeter-wave and THz frequency bands [5]-[6]. For these purposes, a single permittivity dielectric lens backed by dielectric resonators (DR) is able to significantly increase the RCS of the given DR coding particles. However, it leads to increasing impedance mismatch and unwanted scattering with increasing the lens size [58]. A particular improvement of this problem was reported in [59], where a 2D Luneburg lens provided better impedance matching to the free-space and the RCS enhancement of 18 dB at a frequency of 6.2 GHz was achieved. At millimeter-wave frequencies, a 40 mm diameter polypropylene dielectric lens with a 1D photonic crystal (PhC) resonator achieved the RCS enhancement of 14 dB in [60]. The exploitation of PhC structures for a passive RFID system may be more beneficial since a 3D printed high-Q PhC resonator tag showed better RCS performance than is expected for the DR resonators at a frequency of 90 GHz, but due to high attenuation loss, the maximum read-out distance was limited only to 8.5 cm [61]. Such a finding can be potentially developed and improved by a combination of a dielectric lens with spatial permittivity distribution, e.g. Luneburg lens, allowed by a low-loss 3D printing technology [42] as proposed in [5]. The concept of this device is depicted in Fig. 2.7.

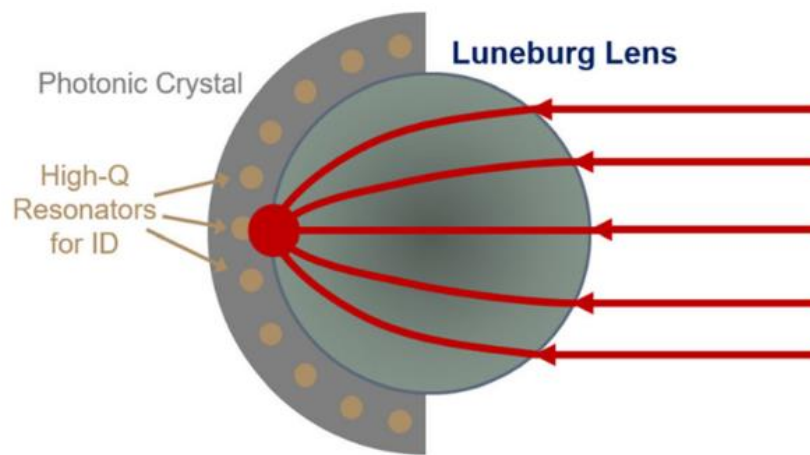


Fig. 2.7 Wide-angle dielectric lens-based retroreflector with frequency-coded high-Q PhC resonators from [5] © 2020, The author(s).

The current challenges of passive, chipless RFID systems at millimeter-wave frequencies and the possibilities of frequency-coding with corner reflectors are summarized in [5]. Then, the advantage of PhC-based tags over DR tags lies in the possibility of using lower permittivity materials ( $\epsilon_r = 9.5$  [42]) instead of very high permittivity materials ( $\epsilon_r = 37$  [58]), which are hardly accessible. Overall, the main drawback of the current solutions is the limited angular coverage, given by the RCS patterns of the used retroreflectors. With further research, both aforementioned disadvantages could be investigated, and novel solutions enabled by a constantly improving additive manufacturing technologies allow for effective designs from millimeter-wave towards THz frequencies.

### 3 Objectives of Thesis

The previous state-of-the-art section of this thesis thoroughly described problems connected with artificial dielectrics and lenses with spatial distribution of the effective EM parameters. The use of effective medium approximations for description of 3D printed dielectric substrates with various inner inclusions patterns is limited. Hence, a precise analytical description can improve the design accuracy and speed up the design process. Therefore, the first objective of the thesis will be:

**Objective 1:** Description of artificial dielectric substrates with selected inclusions by an analytical modelling based on the parallel plate capacitor method.

The parallel plate capacitor method will be exploited to describe the effective permittivity by a diagonal tensor, including the dielectric losses of the real materials. The selected arrangement of inclusions will be described by a single unit cell and analytical models involving its actual physical shape. A dielectric anisotropy will be determined for the case with covering dielectric lids, i.e. creating a dielectric substrate, and without covering lids, in a wide permittivity range of available materials in 3D printing technologies. Various discretization schemes with serial, parallel, or serio-parallel capacitor networks will be evaluated. These models will be further compared to the selected effective medium approximations, and their accuracy will be validated by numerical simulations and measurements.

Since artificial substrates containing conductive and dielectric inclusions have a large potential of the effective constitutive parameters tunability, the second objective of this thesis will be:

**Objective 2:** Description of artificial substrates containing conductive inclusions by an analytical (hybrid) method and determination of their effective constitutive parameters by the multi-modal transfer matrix method.

At this objective, the multi-modal transfer matrix method will be explored for their determination of a selected 3D printed artificial substrate structure. The tunability range of the effective permittivity and the effective permeability will be studied, including the conductivity effect of metallic inclusions. The results achieved will be validated by numerical simulations and measurements of a fabricated sample.

Thanks to the possibilities of 3D printing technologies, lenses with spatial distribution of the effective permittivity have the potential to enhance the performance of passive, chipless RFID systems based on frequency-coding identification. Therefore, attention will be focused on those lenses and exploitation of the QCTO, hence the third objective will be:

**Objective 3:** The research of lenses with spatial distribution of the effective permittivity for retroreflective and frequency-coded retroreflective structures, which allow wide angular coverage and stable RCS.

The capability of the classical and the QCTO modified Luneburg lenses will be assessed in order to increase the RCS and hereby the maximum readout distance of self-localization tag landmarks at millimeter-wave and sub-THz frequencies. Further, investigation of increasing maximum detection angle by the QCTO-enabled design and the possible integration with retroreflective structures to improve overall compactness will be examined.

## 4 State-of-the-Work

In this section, the selected publications of the author are discussed and their contribution to the field of scientific research is evaluated. The achieved results are summarized, and their potential improvements are suggested for future investigation.

### 4.1 Objective 1

The first objective of the thesis deals with the description of artificial dielectric substrates with selected inclusions by an analytical modelling based on the parallel plate capacitor (PPC) method. The goal is to analyze a selected unit cell by the PPC method for different relative permittivities that possess available 3D printing materials. Further investigation is focused on the selection of discretization schemes, i.e. equivalent capacitor networks arranged in vertical, horizontal, or combined direction for different relative permittivity values. The unit cell is chosen to be a cross that is composed of three rods and is often exploited in structures with spatial permittivity distribution, e.g. dielectric lenses. Because the cross is also symmetric, and thus, assuming that it is isotropic, by creating a dielectric substrate from it, the structure will become uniaxially anisotropic.

Therefore, the following questions are as follows:

- How good is the PPC method to include the anisotropy effect in the principal polarization directions?
- How are the effective medium theory approximations (EMAs) accurate to predict the effective relative permittivity during the inclusions volume fraction change compared to the PPC method?
- Is it possible to determine the dielectric losses of the structure by the PPC method?

The research published in Paper [A] answers the first two questions, with conclusions that the anisotropy effect can be precisely determined for low permittivity materials, together with the use of the vertical discretization scheme in the large inclusions volume fraction range. However, for high permittivity materials ( $\epsilon_r > 30$ ), and higher inclusions volume fractions ( $V_i > 0.6$ ), the discrepancy increases, and the combination of vertical and horizontal discretization may be preferred. The reason for this is that the electric energy density over the unit cell is distributed more homogeneously, and thus the polarization effect inside the structure cannot be described only by one dominant discretization direction. Further, the PPC method outperformed the results obtained by the commonly used EMAs in the largest inclusions volume fraction range. The PPC method can be feasible for a relatively accurate and fast estimation of the effective relative permittivity of the artificial dielectric structures whose geometrical and dielectric properties are parametrized.

The future work in this area can be related to the connection of the PPC method with multi-objective optimization and machine learning techniques, where the suitable unit cell geometries showing targeted effective permittivity will be searched out. Also, further continuation may be in the analytical model derivation of the unit cells with tilted walls, showing biaxially anisotropic behavior, e.g. hexagonal or triangular unit cells.

**PhD student's contribution:** The PhD student derived the closed-form effective relative permittivity equations of the unit cell with a cross shaped dielectric inclusion with and without covering lids. Further, he evaluated the effective relative permittivity of the investigated structures numerically in CST Studio Suite and compared those results with the data obtained

from the derived closed-form equations and the ones obtained by the common EMAs approach. Finally, he evaluated the dielectric anisotropy of the investigated structures and the relative errors. The co-authors conducted the effective permittivity measurements and supervised the research and the paper.

The Paper [B] answers the third question related to the determination of an artificial dielectric substrate dielectric losses. The PPC models for the cross-based unit cell are now treated as sub-capacitors with a complex capacitance, which is based on the complex permittivity measurements at the studied frequency range. In this case, the PPC method is able to predict both the effective relative permittivity and the effective dielectric losses for the given inclusions volume fraction and the polarization direction. To verify the results obtained from the PPC-based models, the measurement method employs  $TE_{011}$  and  $TM_{010}$  mode resonators that are suitable for measurement of uniaxial anisotropy. In addition, eigenmode analysis with dielectric losses calculation was exploited. For measurements, both resonators were first fabricated, and the transmission coefficients of the empty cavity resonators were compared with the numerical simulations and matched to include the effects of the surface roughness of the walls, the effective diameter of the resonators, and the coupling of the excitation loops. In the second step, the samples of the cross-based artificial dielectric substrate were 3D printed from a low relative permittivity material (PLA) and then inserted into resonators at the specific position to obtain the transmission coefficients. The measured results were matched to the simulated ones using solid samples with equivalent effective parameters. Finally, a very good agreement was achieved, verifying the ability of the PPC method to precisely determine the effective complex permittivity.

The future work can be focused on the measurements of high-permittivity materials that allow for a larger tunability range of effective complex permittivity.

**PhD student's contribution:** The PhD student implemented two resonators method for effective complex permittivity and anisotropy evaluation of an artificial dielectric substrate based on a cross unit cell. Further, he applied the PPC predictive models for the given unit cell, which he verified by numerical simulations based on dispersion analysis and measurements realized in two resonators. Finally, he evaluated the dielectric anisotropy and relative errors. The co-author 3D printed the artificial dielectric substrate samples and supervised the research and the paper.

## 4.2 Objective 2

The second objective of this dissertation is related to the description of artificial substrates containing conductive inclusions by an analytical (hybrid) method that determines their effective constitutive parameters, i.e. the effective complex permittivity and effective complex permeability. The multi-modal transfer matrix method (MMTMM) binds the voltages, currents and scattering parameters on the wave ports placed on the boundaries of an examined structure via the Bloch's theorem. The goal of this thesis is to determine the effective relative permittivity and effective relative permeability of an artificial substrate containing metallic inclusions. For this study, a self-supporting metallic inclusion based on four crossing rods and dielectric covering lids is selected.

Based on the chosen configuration of the structure, the following research questions arisen:

- What will happen if the dielectric lids are removed and only a fully metallic structure is presented to the propagating EM wave?

- How accurate are the results obtained by the MMTMM compared to the numerical simulations?
- What is the tunability range of the effective constitutive parameters that can be achieved?
- How accurate is the MMTMM compared to the measurements?

The research presented in Paper [C] answers the aforementioned questions and comes with the following conclusions. The fully metallic core of the novel proposed unit cell configuration presents an electromagnetic bandgap (EBG) to the propagating EM wave with relatively high cut-off frequency, depending on the unit cell size. When the dielectric lids are added, propagation of the fundamental quasi-TEM mode is allowed and the proposed artificial substrate exhibits effective permittivity and permeability, which are tunable in wide range depending on the ratio between metallic and dielectric parts, e.g. the effective relative permittivity and the effective relative permeability can vary between 4.5 and 14.5, and 0.69 and 0.24, respectively. The results obtained from the MMTMM agree very well with the numerical simulations performed in the free-space environment, assuming TEM wave propagation. The numerical simulations performed in the enclosed waveguide environment then show a slightly larger difference in the effective relative permittivity value, which is caused by the cosine E-field distribution in the rectangular waveguide. The measurement results were obtained by the waveguide method, which is affected by this non-ideal E-field distribution using the Nicolson-Ross-Weir (NRW) algorithm, and thus the effective relative permittivity was slightly higher, as expected. Nevertheless, the effective relative permeability agreed very well with simulations. The experimental part of this work verified for the first time the applicability of the MMTMM for artificial substrates with metallic inclusions.

The future development of the MMTMM can be focused on the artificial EM structures based on the hexagonal, or triangular arrangement that are fully metallic, or dielectric.

**PhD student's contribution:** The PhD student implemented the hybrid MMTMM and performed its evaluation on an artificial dielectric substrate with a self-supporting conductive inclusion. Further, he metallized the SLA 3D printed sample by a conductive nickel spray and compared the simulated results obtained from the free-space and waveguide environment using the NRW algorithm with the measurement. The co-author 3D printed the sample, conducted measurement in the waveguide by the transmission/reflection method, and supervised the research and the paper.

### 4.3 Objective 3

The third objective of this dissertation is focused on the improvement of the wide angular coverage and stable radar cross section (RCS) response leading to an increased maximum readout distance of the passive, chipless millimeter-wave and sub-THz frequency-coded retroreflectors. To do so, a Luneburg lens which has a variable spatial permittivity profile is a good candidate for this purpose. The transformation of the spherical EM wave into planar EM wave and vice versa is a desirable property of this lens since this functionality can be exploited for retroreflection, particularly frequency-coded by high-Q resonators placed behind the lens, and thus enabling passive ranging and sensing. Also, the Luneburg lens shows a reduced parasitic scattering due to gradient permittivity profile matched to the free-space environment, and the affordable required effective permittivity values are easily accessible by exploiting effective medium theory in 3D printing technologies, making its fabrication cost-effective.

The questions related to this problem are:

- What angular range of the Luneburg lens retroreflector can be achieved at millimeter-wave frequencies and how is its RCS comparable to the conventional radar retroreflectors, which are commonly used as a frequency-coding surface?
- How good is the angular and detection performance of the frequency-coded retroreflector based on the resonators in a photonic crystal (PhC) medium?
- What are the limits of the Luneburg lens exploitation at millimeter-wave and sub-THz frequencies employing 3D printing and other fabrication technologies?
- How can the overall compactness of the Luneburg lens with the coding part be improved? Can it be integrated as a monolithic device without losing its functionality?

The research published in Paper [D] presents the angular performance of the Luneburg lens retroreflector backed with aluminum foil at a millimeter-wave frequency of 80 GHz. The angular range achieved with almost stable RCS performance is  $\pm 75^\circ$  what outperforms a classical dihedral and trihedral corner reflectors that have high RCS in the limited angular range around  $\pm 45^\circ$ . Since the Luneburg lens has a spherical profile, the achievable 3D field of view (FoV) is another advantage over the classical retroreflectors which can work only in their principal planes. However, high precision in lens fabrication and low roughness of the reflective surface are required to avoid unwanted ripples in monostatic RCS characteristics.

When the metallic reflective surface is replaced by the PhC frequency-coding medium created from high-Q dielectric resonators, coupling rod antennas, and low-loss materials, the energy reradiated from the resonators through the Luneburg lens back to the reading antenna creates a long tail response in the time-domain, which can be easily filtered out by properly selected time-gating windows resulting in the frequency-domain detection. Also, multi-bit detection, i.e. detection of multiple devices by angle of arrival (AoA) sensing method is possible. Additionally, the magnitude of the received signal can be used for the distance measurements, enabling ranging functionality. The Luneburg lens with a diameter of 25 mm provides an improvement in read-out distance from 20 cm (single coding particle) to more than 1.2 meters with the use of Rogers RT/Duroid 5880, and more than 4 meters with the use of alumina ceramics [62].

**PhD student's contribution:** The PhD student designed a 3D Luneburg lens with spatially distributed permittivity from stacked perforated dielectric substrate layers which he numerically verified as an antenna and retroreflector by simulations at millimeter-wave frequencies (W-band). Further, he prepared fabrication data for the drilling machine and compared the measured results with the simulated ones. He wrote the major part of the paper related to the performance of the lens and frequency uncoded retroreflector. The co-authors fabricated the lens and performed a characterization of the frequency-coded tag landmark, lens antenna radiation patterns, monostatic RCS patterns, materials characterization, and supervised the research and the paper.

The limits of the Luneburg lens exploitation at millimeter-wave frequencies (W-band) are described in Paper [E], where the stereolithography (SLA) 3D printed Luneburg lens made by a cross unit cell is investigated and the lens parameters degradation (maximum operational frequency, side-lobe levels (SLLs)) caused by the dispersion properties are elaborated. The main frequency limitations are the unit cell size, which is defined by the printing resolution of the 3D printer (higher is better) and the maximum relative permittivity of the material used (lower is better). The major effect of the dispersion is in the lens gain reduction, whereas the effect on SLLs change is negligible. The comparison to the conventional computer numerical control (CNC) machining fabrication performed in Paper [D] is also performed, which showed that the classical fabrication methods may still outperform the modern 3D printing approach in the time and functional parameters costs.

**PhD student's contribution:** The PhD student designed a 3D Luneburg lens with spatially distributed permittivity from the cross unit cells and evaluated the lens performance by numerical simulations at millimeter-wave frequencies (W-band). Further, he prepared the fabrication files and compared the achieved results with the Luneburg lens realized in Paper [D]. The co-author fabricated the designed lens by an SLA 3D printing, conducted the lens antenna characterization, and supervised the research and the paper.

Further, the suitability of a planar Luneburg lens design made from high-resistive silicon (HR-Si) for sub-THz frequencies in the range between 220 GHz and 330 GHz is corroborated in Paper [F]. This paper deals with both the planar Luneburg lens and the wide-angle frequency-coded retroreflector with high-Q resonators embedded in the PhC medium. First, a 20 mm diameter Luneburg lens realized on the 200  $\mu\text{m}$  thin very low-loss HR-Si wafer allowed an increased detection range over 30 cm compared to a few cm without the lens configuration. Second, the lens functionality enabled a wide angular range of  $\pm 65^\circ$  for the coding particles. The fundamental  $\text{TE}_0$  propagation mode in the lens is middle dispersive which is advantageous for covering the whole targeted frequency band with bandwidth over 110 GHz which can be exploited in future 6G communications for high throughput data rates. The frequency limits are again determined by the unit cell size, which depends on the mechanical stability of the walls and the minimum hole diameter achievable by the deep reactive ion etching (DRIE) manufacturing technology used. The disadvantage of the design may be increased fragility.

**PhD student's contribution:** The PhD student designed a planar Luneburg lens which can be realized on a very thin and very low-loss HR-Si dielectric wafer in the sub-THz band (220 GHz–330 GHz). Further, he verified the lens performance by numerical simulations and prepared the data for lens fabrication. He used a rescaled PhC frequency-coding tag for integration with the lens model and verified its functionality by simulations. He wrote the major part of the paper related to the lens design, its numerical simulations, and comparison with the measured data. The co-authors fabricated the designed structures separately for individual characterization, conducted lens antenna parameter measurements, frequency-coding tag landmark characterization, and supervised the research and the paper.

Since the current designs required to be composed of some focusing device, such as a lens, and coding particle, such as resonators, separately, the new approach of mutual integration was first proposed in Paper [G], where the concept of quasi-conformal transformation optics (QCTO) based flattened Luneburg lens backed by the 3D PhC with high-Q resonators is proposed. A very large simulated angular range of  $\pm 87^\circ$  is achieved assuming a high-permittivity material ( $\epsilon_r = 17.5$ ) while the detection of the PhC coding particle is possible up to an angle of  $\pm 75^\circ$ , depending on the coupling position at the bottom of the lens. The proposed combination shall improve the compactness of the whole frequency-coded retroreflector because the coding particles will be integrated with the lens surface. However, for practical realization by 3D printing technique and monolithic integration, only one material with the same relative permittivity can be used. For the proper functionality and maintaining the compact size of the coding PhC part, alumina ceramic with high permittivity ( $\epsilon_r = 9.5$ ) is selected as the reference material.

**PhD student's contribution:** The PhD student proposed a novel concept of a passive, chipless frequency-coded retroreflective identification tag landmark based on a QCTO Luneburg lens with flattened bottom and a 3D PhC with coding resonators, which improves the overall compactness of the identification tag landmark. Further, he evaluated the lens performance by numerical simulations at millimeter-wave frequencies (W-band). The co-authors designed the 3D PhC coding part, performed high performance numerical simulations of the whole identification tag landmark, and supervised the research and the paper.

Due to the reason that the permittivity profile of the QCTO Luneburg lens has to be adjusted accordingly to match the permittivity of alumina, which is used for the PhC coding part, a novel design is proposed in the following Paper [H]. The relation between the maximum beam-steering capabilities of the QCTO Luneburg lens and the maximum relative permittivity value is elaborated with the conclusions that the maximum permittivity provided by alumina allows for the beam-steering range of  $\pm 70^\circ$ . Further, the effects of real capabilities and restrictions of lithography-based ceramics manufacturing (LCM) 3D printing on the lens performance are evaluated. Since the study on the broadband impedance matching layers (IML) in [54] was conducted assuming the maximum relative permittivity of 2.9, the effects of using different broadband IMLs to the free-space environment on the antenna gain and impedance matching were investigated, assuming a maximum available relative permittivity of 8.9. In our work, the best results are achieved for the exponential IML, while in [54], the best results were achieved for the Klopfenstein IML. The performance of the designed QCTO Luneburg lens is successfully verified by the measurements at a frequency of 40 GHz as a lens antenna and a metal backed retroreflector, which was firstly evaluated in this extensive work.

**PhD student's contribution:** The PhD student proposed a flattened 3D QCTO Luneburg lens with a permittivity profile adjusted to the alumina for LCM and created MATLAB codes for generation of its simplified and full fabrication models in CST Studio Suite at millimeter-wave frequencies (Ka-band). Further, he designed and, by numerical simulations, evaluated different broadband IMLs profiles to improve overall impedance matching of the lens permittivity profile to the free-space environment. He also simulated the performance of the designed lens as a retroreflector when its bottom surface is backed by a reflective layer. In addition, he described the effects of non-ideal fabrication process on the lens antenna performance and compared the measured results to the simulations. The co-authors helped with the calculation of the adjusted QCTO Luneburg lens relative permittivity profile in COMSOL Multiphysics, fabricated the lenses with and without IML by a ceramic 3D printing process, measured the lens antenna radiation patterns, conducted the monostatic RCS measurements of the retroreflector, and supervised the research and the paper.

The future integration of the QCTO Luneburg lens with the 3D PhC coding part requires ensuring the impedance matching between the bottom lens permittivity profile and the PhC effective permittivity profile, especially the impedance of the input PhC waveguides, for maximizing the transmitted and reflected power. Thereafter, the monolithic configuration of the whole device will be possible. In addition, the dependence of the frequency-coded retroreflector functionality over the high temperature range (e.g. in case of fire) will be evaluated together with the maximum frequency achievable in the current design. Currently, unpublished results verify that the operation is possible up to a frequency of 95 GHz and a temperature over 900 °C. The results are intended to be summarized and submitted for publication in the near future.

## 5 Conclusions and Future Work

The dissertation thesis dealt with the research of 3D printed artificial electromagnetic structures containing dielectric and metallic inclusions of various geometries that could be exploitable for antenna and microwave component design. During this research, three main objectives were formulated and gradually solved.

The first objective of the thesis was focused on the description of artificial dielectric substrates with selected inclusions by an analytical modelling based on the PPC method. The following original results were achieved:

- Derivation of closed-form equations for effective relative permittivity determination of an artificial dielectric substrate based on a cross unit cell that outperforms conventional EMAs in the wide inclusions volume fraction range Paper [A].
- Determination of the dielectric losses of the artificial dielectric substrate based on the cross unit cell Paper [B].

The second objective of the thesis was focused on the description of artificial substrates containing conductive inclusions by an analytical (hybrid) method and determination of their effective constitutive parameters by the MMTMM. The following original results were achieved and published in Paper [C]:

- Determination of the effective relative permittivity and effective relative permeability of a self-supporting unit cell by the MMTMM and evaluation of their ranges for varying sizes of conductive inclusion.
- Description of the influence of the finite conductivity of the inclusions on the effective constitutive parameters.

The third objective of the thesis was related to the research of lenses with spatial distribution of the effective permittivity for retroreflective and frequency-coded retroreflective structures, which allow wide angular coverage and stable RCS. The following original results were achieved:

- A 3D Luneburg lens realized at millimeter-wave frequencies (W-band) from stacked substrate layers using CNC drilling serving as an antenna or a wide-angle retroreflector with a stable RCS in an angular range of  $\pm 75^\circ$  Paper [D].
- Experimental validation of wide-angle detection with stable RCS and maximum detection range enhancements using Luneburg lenses with passive, chipless frequency-coded RFID tag landmarks Papers [D, F].
- A 3D Luneburg lens realized at millimeter-wave frequencies (W-band) from cross unit cells using SLA 3D printing, limitations and comparison to CNC drilled version of the lens Paper [E].
- A 2D Luneburg lens realized at millimeter-wave frequencies (220–330 GHz frequency band) from a perforated HR-Si wafer using DRIE and its integration with rescaled PhC coding tag for passive, chipless frequency-coded RFID Paper [F].
- A novel concept that combines the 3D QCTO-based flattened Luneburg lens with a 3D PhC coding medium for integrated wide-angle passive, chipless frequency-coded RFID tag landmarks Paper [G].
- A 3D QCTO-based Luneburg lens realized at millimeter-wave frequencies (Ka-band) from cross unit cells using LCM 3D printing evaluated as an antenna and firstly as a retroreflector Paper [H].

Considering the achieved results, it is apparent that all the objectives of this thesis were successfully accomplished.

The future research direction related to artificial dielectrics can be in the evaluation of inverse design topology optimization [63], multi-objective optimization [64], and deep learning methods [65] that would create a spatial composition of the structure according to the requirements given by the input parameters. Furthermore, the study of various 3D EM structures involving conductive and/or dielectric inclusions in various supercell and lattice configurations, together with higher symmetries, which have shown promising results for the enhancements of operational bandwidths of various microwave and antenna structures [30], can be in the future focus of researchers.

The next development of GRIN lenses and retroreflectors with coding parts can be seen in enabling continuous tuning capabilities, which are very demanding in the next era of 6G communications systems, especially in combination with the development of low-loss materials and fast, cost-efficient manufacturing techniques. Therefore, the future research target can involve a lower temperature sintering ceramic 3D printing process [66] to design GRIN lenses with a lower permittivity gradient that can increase the maximum operational frequency. Further, the continuous tunability enabled by the use of liquid crystal (LC) technology, or development of reconfigurable / functional materials allow novel devices with tunable functionalities to be explored.

# Bibliography

- [1] S. Ford and M. Despeisse. Additive manufacturing and sustainability: an exploratory study of the advantages and challenges. *Journal of Cleaner Production*. **137**:1573–1587, Nov. 2016. doi: 10.1016/j.jclepro.2016.04.150.
- [2] A. Sihvola. Mixing Rules with Complex Dielectric Coefficients. *Subsurface Sensing Technologies and Applications*. **1**(4):395–415, Oct. 2000. doi: 10.1023/A:1026511515005.
- [3] M. Y. Koledintseva, S. K. Patil, R. W. Schwartz, W. Huebner, K. N. Rozanov, J. Shen and J. Chen. Prediction of Effective Permittivity of Diphasic Dielectrics as a Function of Frequency. *IEEE Transactions on Dielectrics and Electrical Insulation*, **16**(3):793–808, Jun. 2009. doi: 10.1109/TDEL.2009.5128520.
- [4] A. C. Escobar, J. P. Del Risco, O. Quevedo-Teruel, F. Mesa and J. D. Baena. Retrieval of the Constitutive Parameters and Dispersion Relation of Glide-Symmetric Metamaterials via the Multimodal Transfer Matrix Method. *2020 Fourteenth International Congress on Artificial Materials for Novel Wave Phenomena (Metamaterials)*, New York, NY, USA, 2020, pp. 312–314, doi: 10.1109/Metamaterials49557.2020.9285093.
- [5] A. Jiménez-Sáez, A. A. Abbas, M. Schüßler, A. Abuelhaia, M. El-Absi, M. Sakaki, L. Samfaß, N. Benson, M. Hoffmann, R. Jakoby, T. Kaiser and K. Solbach. Frequency-Coded mm-Wave Tags for Self-Localization System Using Dielectric Resonators. *Journal of Infrared, Millimeter and Terahertz Waves*, **41**(3):908–925, Aug. 2020, doi: 10.1007/s10762-020-00707-0.
- [6] M. El-Absi, A. Alhaj Abbas, A. Abuelhaija, F. Zheng, K. Solbach and T. Kaiser. High-Accuracy Indoor Localization Based on Chipless RFID Systems at THz Band. *IEEE Access*, **6**:54355–54368, Sep. 2018. doi: 10.1109/ACCESS.2018.2871960.
- [7] G. A. R. Arroyave and J. L. A. Quijano. Broadband Characterization of 3D Printed Samples with Graded Permittivity. *2018 International Conference on Electromagnetics in Advanced Applications (ICEAA)*, Cartagena, Colombia, 2018, pp. 584–588. doi: 10.1109/ICEAA.2018.8520349.
- [8] M. Mrnka and Z. Raida. An Effective Permittivity Tensor of Cylindrically Perforated Dielectrics. *IEEE Antennas and Wireless Propagation Letters* **17**(1):66–69, Jan. 2018. doi: 10.1109/LAWP.2017.2774448.
- [9] J. Machac. Microstrip line on an artificial dielectric substrate. *IEEE Microwave and Wireless Components Letters*, **16**(7):416–418, Jul. 2006. doi: 10.1109/LMWC.2006.877120
- [10] C. C. Njoku, W. G. Whittow and J. C. Vardaxoglou. Simulation Methodology for Synthesis of Antenna Substrates With Microscale Inclusions. *IEEE Transactions on Antennas and Propagation*, **60**(5):2194–2202, May 2012. doi: 10.1109/TAP.2012.2189736.
- [11] A. Knisely, M. Havrilla and P. Collins. Biaxial anisotropic sample design and rectangular to square waveguide material characterization system. *2015 9th International Congress on Advanced Electromagnetic Materials in Microwaves and Optics (METAMATERIALS)*, Oxford, UK, 2015, pp. 346–348. doi: 10.1109/MetaMaterials.2015.7342445.
- [12] Z. Manzoor, M. T. Ghasr and K. M. Donnell. Microwave characterization of 3D printed conductive composite materials. *2018 IEEE International Instrumentation and Measurement Technology Conference (I2MTC)*, Houston, TX, USA, 2018, pp. 1–5. doi: 10.1109/I2MTC.2018.8409627.
- [13] P. I. Dankov. Characterization of Dielectric Properties, Resultant Isotropy and Anisotropy of 3D Printed Dielectrics. *2018 48th European Microwave Conference (EuMC)*, Madrid, Spain, 2018, pp. 823–826. doi: 10.23919/EuMC.2018.8541621.
- [14] S. Muller, P. Scheele, C. Weil, M. Wittek, C. Hock and R. Jakoby. Tunable passive phase shifter for microwave applications using highly anisotropic liquid crystals. *2004 IEEE MTT-S International Microwave Symposium Digest (IEEE Cat. No.04CH37535)*, Fort Worth, TX, USA, 2004, pp. 1153–1156. doi: 10.1109/MWSYM.2004.1339190.
- [15] E. Drake, R. R. Boix, M. Horno and T. K. Sarkar. Effect of substrate dielectric anisotropy on the frequency behavior of microstrip circuits. *IEEE Transactions on Microwave Theory and Techniques*, **48**(8):1394–1403, Aug. 2000. doi: 10.1109/22.859486.

- [16] C. D. Morales, C. Morlaas, A. Chabory, R. Pascaud, M. Grzeskowiak and G. Mazingue. 3D-printed ceramics with engineered anisotropy for dielectric resonator antenna applications. *Electronics Letters*, **57**(17):679–681, Aug. 2021. doi: 10.1049/ell2.12234.
- [17] K. F. Brakora, J. Halloran and K. Sarabandi. Design of 3-D monolithic MMW antennas using ceramic stereolithography. *IEEE Transactions on Antennas and Propagation*, **55**(3):790–797, Mar. 2007. doi: 10.1109/TAP.2007.891855.
- [18] V. A. Markel, Introduction to the Maxwell Garnett approximation: tutorial. *Journal of the Optical Society of America A*, **33**(7):1244–1256, Jun. 2016. doi: 10.1364/JOSAA.33.001244.
- [19] M. Johansson, C. L. Holloway and E. F. Kuester. Effective electromagnetic properties of honeycomb composites, and hollow-pyramidal and alternating-wedge absorbers. *IEEE Transactions on Antennas and Propagation*, **53**(2):728–736, Feb. 2005. doi: 10.1109/TAP.2004.841320.
- [20] J. Ji, Y. Ma and Y. Wang. Inclusion's distribution pattern's influence on mixture's effective permittivity in two dimension utilizing finite difference method (FDM). *Optik*, **200**:163384, Jan. 2020. doi: 10.1016/j.ijleo.2019.163384.
- [21] S. Torquato and S. Hyun. Effective-medium approximation for composite media: Realizable single-scale dispersions. *Journal of Applied Physics*, **89**(3):1725–1729, Jan. 2001, doi: 10.1063/1.1336523.
- [22] S. Zhang, W. Whittow and J. C. Vardaxoglou. Additively manufactured artificial materials with metallic meta-atoms. *IET Microwaves, Antennas & Propagation*, **11**(14):1955–1961, Nov. 2017. doi:10.1049/iet-map.2016.0952.
- [23] T. Whittaker, W. Whittow and J. Y. C. Vardaxoglo. Meta-atom loaded patch antenna. *The Loughborough Antennas & Propagation Conference (LAPC 2018)*, Loughborough, 2018, pp. 1–2, doi: 10.1049/cp.2018.1460.
- [24] T. W. Whittaker, W. G. Whittow and J. C. Vardaxoglou. Artificially Engineered Capacitors for Discrete High-Frequency Electronic Circuitry. *IEEE Transactions on Microwave Theory and Techniques*, **68**(1):74–86, Jan. 2020. doi: 10.1109/TMTT.2019.2950224.
- [25] Y. Jarmoumi, A. Derouiche and F. Benzouine. A New Numerical-Homogenization Method to Predict the Effective Permittivity of Composite Materials. *Integrating Materials and Manufacturing Innovation*, **9**:423–434, Dec. 2020. doi: 10.1007/s40192-020-00194-0.
- [26] Y. Feldman, Y. A. Gusev and M. A. Vasilyeva. Dielectric relaxation phenomena in complex systems. Tutorial, Kazan University, Kazan, 2012.
- [27] A. G. Knisely. Biaxial Anisotropic Material Development and Characterization using Rectangular to Square Waveguide. M.Sc. thesis, Air Force Institute of Technology, OH, USA, 2015.
- [28] F. Mesa, R. Rodriguez-Berral and F. Medina. Unlocking Complexity Using the ECA: The Equivalent Circuit Model as An Efficient and Physically Insightful Tool for Microwave Engineering. *IEEE Microwave Magazine*, **19**(4):44–65, Jun. 2018. doi: 10.1109/MMM.2018.2813821.
- [29] A. C. Escobar, J. P. Del Risco, O. Quevedo-Teruel, F. Mesa and J. D. Baena. Retrieval of the Constitutive Parameters and Dispersion Relation of Glide-Symmetric Metamaterials via the Multimodal Transfer Matrix Method. *2020 Fourteenth International Congress on Artificial Materials for Novel Wave Phenomena (Metamaterials)*, New York, NY, USA, 2020, pp. 312–314. doi: 10.1109/Metamaterials49557.2020.9285093.
- [30] F. Mesa, G. Valerio, R. Rodriguez-Berral and O. Quevedo-Teruel. Simulation-Assisted Efficient Computation of the Dispersion Diagram of Periodic Structures: A Comprehensive Overview With Applications to Filters, Leaky-Wave Antennas and Metasurfaces. *IEEE Antennas and Propagation Magazine*, **63**(5):33–45, Oct. 2021. doi: 10.1109/MAP.2020.3003210.
- [31] D. M. Pozar. *Microwave Engineering*, 4<sup>th</sup> ed., Wiley, 2011, ISBN 978-0-470-63155-3.
- [32] F. Giusti, F. Mesa, Q. Chen, G. Valerio and O. Quevedo-Teruel. Multimodal Transfer Matrix Method Applied to 3-D Periodic Structures. *2021 International Symposium on Antennas and Propagation (ISAP)*, Taipei, Taiwan, 2021, pp. 1–2. doi: 10.23919/ISAP47258.2021.9614393.
- [33] S. Yang, F. Mesa, O. Zetterstrom, S. Clendinning and O. Quevedo-Teruel. Understanding the Dispersion Diagrams of Two-Dimensional Supercells. *2022 Microwave Mediterranean Symposium (MMS)*, Pizzo Calabro, Italy, 2022, pp. 1–4. doi: 10.1109/MMS55062.2022.9825507.

- [34] F. Zheng and P. Zhang. Phonon Unfolding: A program for unfolding phonon dispersions of materials. *Computer Physics Communications*, **210**:139–144, Jan. 2017. doi: 10.1016/j.cpc.2016.09.005.
- [35] A. Aziz, L. Matekovits and A. D. Sabata. A simple and robust technique to retrieve effective refractive index of heterogeneous dielectrics for millimeter-wave applications. *2015 Computational Electromagnetics International Workshop (CEM)*, Izmir, Turkey, 2015, pp. 1–2. doi: 10.1109/CEM.2015.7237420.
- [36] W. B. Weir. Automatic measurement of complex dielectric constant and permeability at microwave frequencies. *Proceedings of the IEEE*, **62**(1):33–36, Jan. 1974. doi: 10.1109/PROC.1974.9382.
- [37] J. Baker-Jarvis, E. J. Vanzura and W. A. Kissick. Improved technique for determining complex permittivity with the transmission/reflection method. *IEEE Transactions on Microwave Theory and Techniques*, **38**(8):1096–1103, Aug. 1990. doi: 10.1109/22.57336.
- [38] D. K. Ghodgaonkar, V. V. Varadan and V. K. Varadan. Free-space measurement of complex permittivity and complex permeability of magnetic materials at microwave frequencies. *IEEE Transactions on Instrumentation and Measurement*, **39**(2):387–394, Apr. 1990. doi: 10.1109/19.52520.
- [39] J. Krupka. Frequency domain complex permittivity measurements at microwave frequencies. *Measurement Science and Technology*, **17**(6):R55–R70, Apr. 2006. doi: 10.1088/0957-0233/17/6/R01.
- [40] J. Zechmeister and J. Lacik. Complex Relative Permittivity Measurement of Selected 3D-Printed Materials up to 10 GHz. *2019 Conference on Microwave Techniques (COMITE)*, Pardubice, Czech Republic, 2019, pp. 1–4. doi: 10.1109/COMITE.2019.8733590.
- [41] Z. Larimore, S. Jensen, A. Good, A. Lu, J. Suarez and M. Mirotznik. Additive Manufacturing of Luneburg Lens Antennas Using Space-Filling Curves and Fused Filament Fabrication. *IEEE Transactions on Antennas and Propagation*, **66**(6):2818–2827, Jun. 2018. doi: 10.1109/TAP.2018.2823819.
- [42] A. Jiménez-Sáez, M. Schüßler, C. Krause, D. Pandel, K. Rezer, G. V. Bögel, N. Benson and R. Jakoby. 3D Printed Alumina for Low-Loss Millimeter Wave Components. *IEEE Access*, **7**:40719–40724, Apr. 2019. doi: 10.1109/ACCESS.2019.2906034.
- [43] *Rogers Corporation. RT/Duroid® 6006 and 6010 LM Laminate Data Sheet*. Accessed on: [12-10-2022]. [Online]. Available: <https://www.rogerscorp.com/-/media/project/rogerscorp/documents/advanced-electronics-solutions/english/data-sheets/rt-duroid-6006-6010lm-laminate-data-sheet.pdf>.
- [44] P. I. Deffenbaugh, T. M. Weller and K. H. Church. Fabrication and Microwave Characterization of 3-D Printed Transmission Lines. *IEEE Microwave and Wireless Components Letters*, **25**(12):823–825, Dec. 2015. doi: 10.1109/LMWC.2015.2495184.
- [45] C.A. Fernandes, E.B Lima and J.R. Costa. Dielectric Lens Antennas. In: Z. Chen (eds) *Handbook of Antenna Technologies*. Springer, Singapore, 2015, ISBN: 978-981-4560-75-7. doi: 10.1007/978-981-4560-75-7\_40-1.
- [46] S. Zhang, D. Cadman and J. Y. C. Vardaxoglou. Additively Manufactured Profiled Conical Horn Antenna With Dielectric Loading. *IEEE Antennas and Wireless Propagation Letters*, **17**(11):2128–2132, Nov. 2018. doi: 10.1109/LAWP.2018.2871029.
- [47] M. A. B. Abbasi, V. F. Fusco, H. Tataria and M. Matthaiou. Constant- $\epsilon_r$  Lens Beamformer for Low-Complexity Millimeter-Wave Hybrid MIMO. *IEEE Transactions on Microwave Theory and Techniques*, **67**(7):2894–2903, Jul. 2019. doi: 10.1109/TMTT.2019.2903790.
- [48] S. Zhang, R. K. Arya, W. G. Whittow, D. Cadman, R. Mittra and J. C. Vardaxoglou. Ultra-Wideband Flat Metamaterial GRIN Lenses Assisted With Additive Manufacturing Technique. *IEEE Transactions on Antennas and Propagation*, **69**(7):3788–3799, Jul. 2021. doi: 10.1109/TAP.2020.3044586.
- [49] C-C. Chen and J. L. Volakis. Bandwidth broadening of patch antennas using nonuniform substrates. *Microwave and Optical Technology Letters*, **47**(5):421–423, Dec. 2005. doi: 10.1002/mop.21189.
- [50] M. Berg, T. Tuovinen and E. Salonen. Artificial anisotropic dielectric material for antenna polarization

- rotation. *2017 Progress In Electromagnetics Research Symposium - Spring (PIERS)*, St. Petersburg, Russia, 2017, pp. 3771–3776. doi: 10.1109/PIERS.2017.8262414.
- [51] J. Chetan. Controlling radiation pattern of patch antenna using Transformation Optics based dielectric superstrate. PhD thesis, Télécom ParisTech, 2016.
- [52] N. Landy, Y. Urzhumov and D. R. Smith. Quasi-Conformal Approaches for Two and Three-Dimensional Transformation Optical Media. In: D. H. Werner and D.-H. Kwon. *Transformation Electromagnetics and Metamaterials*, pp. 1–32, 2013. doi: 10.1007/978-1-4471-4996-5\_1.
- [53] L. Wu, X. Tian, H. Ma, M. Yin and D. Li. Broadband flattened Luneburg lens with ultra-wide angle based on a liquid medium. *Applied Physics Letters*, **102**(7), At. no. 074103, Feb. 2013. doi: 10.1063/1.4793206.
- [54] S. Biswas and M. Mirotznik. High gain, wide-angle QCTO-enabled modified Luneburg lens antenna with broadband anti-reflective layer. *Scientific Reports*, **10**, Art no. 12646, Jul. 2020. doi: 10.1038/s41598-020-69631-6.
- [55] H. Haddad. Reflection control techniques of a plane wave using transformation optics and surface impedance modulation – Application to the flattening of the retro-directive reflector. PhD thesis, Université Libanaise - Liban, 2018.
- [56] L. Liang and S. V. Hum. Wide-angle scannable reflector design using conformal transformation optics. *Optics Express*, **21**(2):2133–2146, Jan. 2013. doi: 10.1364/OE.21.002133.
- [57] R. A. Bahr, A. O. Adeyeye, S. Van Rijs and M. M. Tentzeris. 3D-Printed Omnidirectional Luneburg Lens Retroreflectors for Low-Cost mm-Wave Positioning. *2020 IEEE International Conference on RFID (RFID)*, Orlando, FL, USA, 2020, pp. 1–7. doi: 10.1109/RFID49298.2020.9244891.
- [58] A. A. Abbas, M. El-Absi, A. Abuelhaija, K. Solbach and T. Kaiser. RCS Enhancement of Dielectric Resonator Tag Using Spherical Lens. *Frequenz: Journal of RF-Engineering and Telecommunications*, **73**(5–6):161–170, Feb. 2019. doi: 10.1515/freq-2018-0224.
- [59] Y. Zhao, J. Weidenmueller, G. Bogel, A. Grabmaier, A. A. Abbas, K. Solbach, A. Jiménez-Sáez, M. Schüßler and R. jakoby. 2D Metamaterial Luneburg Lens for Enhancing the RCS of Chipless Dielectric Resonator Tags. *2019 Second International Workshop on Mobile Terahertz Systems (IWMTS)*, Bad Neuenahr, Germany, 2019, pp. 1–6. doi: 10.1109/IWMTS.2019.8823784.
- [60] A. A. Abbas, Y. Zantah, K. Solbach and T. Kaiser. Frequency-Coded Lens by Photonic Crystal Resonator for mm-Wave Chipless RFID Applications. *2021 Fourth International Workshop on Mobile Terahertz Systems (IWMTS)*, Essen, Germany, 2021, pp. 1–5. doi: 10.1109/IWMTS51331.2021.9486828.
- [61] A. Jiménez-Sáez, M. Schüßler, D. Pandel, N. Benson and R. Jakoby. 3D Printed 90 GHz Frequency-Coded Chipless Wireless RFID Tag. *2019 IEEE MTT-S International Microwave Workshop Series on Advanced Materials and Processes for RF and THz Applications (IMWS-AMP)*, Bochum, Germany, 2019, pp. 4–6. doi: 10.1109/IMWS-AMP.2019.8880140.
- [62] A. Jiménez-Sáez. Towards THz Chipless High-Q Cooperative Radar Targets for Identification, Sensing, and Ranging. Springer Theses, 2022. ISBN: 9783031049750.
- [63] M. Otomori, J. Andkjaer, O. Sigmund, K. Izui and S. Nishiwaki. Inverse design of dielectric materials by topology optimization. *Progress In Electromagnetics Research*, **127**:93–130, Apr. 2012. doi: 10.2528/PIER12020501.
- [64] S. D. Campbell, D. Sell, R. P. Jenkins, E. B. Whiting, J. A. Fan and D. H. Werner. Review of numerical optimization techniques for meta-device design [Invited]. *Optical Materials Express*, **9**(4):1842–1863, Mar. 2019. doi: 10.1364/OME.9.001842.
- [65] Y. Sharma, X. Chen, J. Wu, Q. Zhou, H. H. Zhang and H. Xin. Machine Learning Methods-Based Modeling and Optimization of 3-D-Printed Dielectrics Around Monopole Antenna. *IEEE Transactions on Antennas and Propagation*, **70**(7):4997–5006, Jul. 2022. doi: 10.1109/TAP.2022.3153688.
- [66] P. E. Parsons. Material development for functional additive manufacturing. PhD thesis, University of Delaware, DE, USA, 2020.

# Selected Publications of the Author

## Objective 1:

- [A] P. Kadera, J. Lacik and H. Arthaber. Effective Relative Permittivity Determination of 3D Printed Artificial Dielectric Substrates Based on a Cross Unit Cell. *Radioengineering*, **30**(4):595–610, Dec. 2021. doi: 10.13164/re.2021.0595.
- [B] P. Kadera and J. Lacik. Effective Complex Permittivity Measurement of 3D Printed Artificial Dielectric Substrate Based on a Cross Unit Cell. *24th International Microwave and Radar Conference (MIKON)*, Gdansk, Poland, 2022, pp. 449–453. ISBN: 978-83-956020-3-0.

## Objective 2:

- [C] P. Kadera and J. Lacik. Effective Constitutive Parameters Retrieval of Artificial 3D Printed Substrates with Conductive Inclusions. *2022 32th International Conference Radioelektronika (RADIOELEKTRONIKA)*, Košice, Slovakia, 2022, pp. 1–4. doi: 10.1109/RADIOELEKTRONIKA54537.2022.9764946.

## Objective 3:

- [D] P. Kadera, A. Jiménez-Sáez, T. Burmeister, J. Lacik, M. Schüßler and R. Jakoby. Gradient-Index-Based Frequency-Coded Retroreflective Lenses for mm-Wave Indoor Localization. *IEEE Access*, **8**:212765–212775, Nov. 2020. doi: 10.1109/ACCESS.2020.3039986.
- [E] P. Kadera and J. Lacik. Performance Comparison of W-band Luneburg Lens Antenna: Additive versus Subtractive Manufacturing. *2021 20th International Conference on Microwave Techniques (COMITE)*, Brno, Czech Republic, 2021, pp. 1–6. doi: 10.1109/COMITE52242.2021.9419879.
- [F] P. Kadera, J. Sánchez-Pastor, L. Schmitt, M. Schüßler, R. Jakoby, M. Hoffmann, A. Jiménez-Sáez and J. Lacik. Sub-THz Luneburg lens enabled wide-angle frequency-coded identification tag for passive indoor self-localization. *International Journal of Microwave and Wireless Technologies*, 1–15, May 2022. doi: 10.1017/S175907872200054X.
- [G] P. Kadera, J. Sánchez-Pastor, A. Jiménez-Sáez, M. Schüßler, J. Lacik and R. Jakoby. QCTO Luneburg Lens-Based Retroreflective Tag Landmarks for mm-Wave Self-Localization Systems. *2021 IEEE-APS Topical Conference on Antennas and Propagation in Wireless Communications (APWC)*, Honolulu, Hawaii, USA, 2021, pp. 105–108. doi: 10.1109/APWC52648.2021.9539571.
- [H] P. Kadera, J. Sánchez-Pastor, H. Eskandari, T. Tyc, M. Sakaki, M. Schüßler, R. Jakoby, N. Benson, A. Jiménez-Sáez and J. Lacik. Wide-Angle Ceramic Retroreflective Luneburg Lens based on Quasi-Conformal Transformation Optics for mm-Wave Indoor Localization. *IEEE Access*, **10**:41097–41111, Apr. 2022. doi: 10.1109/ACCESS.2022.3166509.

# Other Publications of the Author

- [I] P. Kadera, A. Jiménez-Sáez, L. Schmitt, M. Schüßler, M. Hoffmann, J. Lacik and R. Jakoby. Frequency Coded Retroreflective Landmark for 230 GHz Indoor Self-Localization Systems. *2021 15th European Conference on Antennas and Propagation (EuCAP)*, Dusseldorf, Germany, 2021, pp. 1–5. doi: 10.23919/EuCAP51087.2021.9410973.
- [J] P. Kadera. Comparison of Measurement Methods for Characterization of 3D Printed Low-Loss Artificial Dielectric Substrate Based on Cross Unit Cell. *Proceedings II of the 27st Conference STUDENT EEICT 2021: Selected papers*, Brno, Czech Republic, 2021, pp. 214–218. ISBN: 978-80-214-5943-4.
- [K] P. Kadera, T. Mikulasek, J. Hruska and J. Lacik. Hyperbolic Lens Horn Antenna for Fixed-Beam E-Band Communication. *2020 30th International Conference Radioelektronika (RADIOELEKTRONIKA)*, Bratislava, Slovakia, 2020, pp. 1–5. doi: 10.1109/RADIOELEKTRONIKA49387.2020.9092359.

# Curriculum Vitae

## Petr Kaděra

Born: 02.02.1994, Čeladná, Czech Republic  
E-mail: petrkadera4@gmail.com

### Education

- 2018–2023 Brno University of Technology, Brno, Czech Republic  
Ph.D., Electronics and Communication Technologies  
Research topic: 3D Printed Artificial Materials for Microwave Structures
- 2016–2018 Brno University of Technology, Brno, Czech Republic  
MSc., Electronics and Communication, graduated with distinction  
Diploma thesis: Horn Antenna with Suppressed Side-Lobe Radiation
- 2013–2016 Brno University of Technology, Brno, Czech Republic  
BSc., Electronics and Communication, graduated with distinction  
Bachelor thesis: Energy Harvesting Demonstrator

### Working experience and research stays

- 10/2022 to 11/2022 Technical University Graz, Graz, Austria, Aktion Österreich-Tschechien  
Visiting PhD student – tunable reflectarray antennas based on liquid crystals
- 10/2021 to 11/2021 KTH Royal Institute of Technology, Stockholm, Sweden  
Visiting PhD student – multi-modal transfer matrix method for metallic/dielectric unit cells in hexagonal arrangement
- 1/2020 to 4/2020 Technical University Darmstadt, Darmstadt, Germany  
Visiting PhD student – millimeter-wave retroreflecting lenses
- 4–5/2022 Visiting PhD student – wide-angle low-temperature ceramic sintering lenses
- 4/2019 to present TESCAN Brno, s.r.o. Brno, Czech Republic  
R&D Intern – detection systems of scanning electron microscopes
- 1/2018 to 5/2018 RACOM, s.r.o. – Nové Město na Moravě, Czech Republic  
Master's thesis solution
- 12/2016 to 12/2017 ERA, a.s. - Brno, Czech Republic  
R&D Intern – microwave characterization of composite materials

### Research projects

- 3/2020 to 12/2022 Advanced high-frequency structures and modeling of electromagnetics problems, project no. FEKT-S-20-6526 (co-investigator)
- 2/2021 to 1/2022 mm-Wave passive indoor localization landmarks based on transformation optics electromagnetics (principal investigator)

OP RDE Quality internal grants of Brno University of Technology, project no. CZ.02.2.69/0.0/0.0/19\_073/0016948

1/2020 to present      Mobile Material Characterization and Localization by Electromagnetic Sensing Deutsche Forschungsgemeinschaft, project no. 287022738, TRR 196 – C09 (team member)

### **Awards**

12/2018      Best Master's thesis in student content (IEEE - MTT/AP/ED/EMC Joint Chapter Czechoslovakia Section)

6/2018      Dean's award for Master's thesis

6/2016      Dean's award for Bachelor's thesis

### **Languages**

Czech          Native

English        B2 level

### **Software skills**

CST Studio Suite, MATLAB, ANSYS Electronics Desktop, Orcad PSpice, KiCad, AWR Microwave Office, Comsol Multiphysics, LabVIEW, MS Office

### **Additional education**

6/2019      European School of Antennas – Loughborough University, United Kingdom  
Advanced Materials for Antennas and Microwave Devices

## Abstract

The dissertation thesis deals with the research of 3D printed artificial electromagnetic structures exploitable for antenna and microwave component design. Artificial structures containing dielectric and metallic inclusions of various geometries are investigated, and their precise description, including the anisotropy effect, can improve the actual design speed and accuracy.

First, the models based on the analytical parallel plate capacitor method are compared with an effective medium theory, numerical, and experimental results, which are provided for various parameters of materials available in 3D printing technology. The proposed models derived by the parallel plate capacitor method can generally be exploited for faster and highly accurate determination of the effective complex permittivity, which enhances its potential to be used with optimization techniques. Second, the hybrid multimodal transfer matrix method is exploited as a general and effective way for calculations of the effective permittivity and effective permeability of artificial structures containing both dielectric and metallic inclusions through the volumetric space of the structures studied. The artificial structures containing metallic inclusions generally allow to achieve a wide tuning range of the effective constitutive parameters.

Finally, suitable structures with spatial permittivity distribution are developed for wide-angle millimeter-wave gradient-index Luneburg lenses employable as antennas or retroreflectors for wide angular coverage and stable radar cross section enhancements of passive, chipless frequency-coded radiofrequency identification tag landmarks which have a large potential for indoor self-localization.

## Abstrakt

Tato dizertační práce se zabývá výzkumem 3D tištěných umělých elektromagnetických struktur pro návrh antén a mikrovlnných obvodů. Umělé struktury obsahující dielektrické i vodivé příměsi s různými geometrickými tvary jsou zkoumány a jejich přesný popis, včetně zahrnutí vlivu anizotropie, může zlepšit stávající přesnost a rychlost návrhu.

Prvně jsou srovnány modely založené na analytickém přístupu modelování kapacitorů s teorií efektivního media, numerickou simulací a naměřenými výsledky, které jsou poskytnuty pro rozličné parametry materiálů, jenž jsou dostupné v technologii 3D tisku. Navržené modely metodou kapacitorů mohou být obecně využity pro rychlejší a přesnější určení efektivní komplexní permitivity, což zvyšuje potenciál dané metody při využití optimalizačních technik. Jako druhá je využita metoda vícemódových přenosových matic, která poskytuje obecný a účinný způsob výpočtu efektivní permitivity a efektivní permeability umělých struktur obsahující jak dielektrické, tak i kovové inkluze, napříč objemovým prostorem zkoumané struktury. Umělé struktury obsahující kovové inkluze obecně umožňují dosahovat široký ladící rozsah efektivních konstitutivních parametrů.

Následně jsou navrženy vhodné struktury s prostorovým rozložením permittivity pro širokoúhlé Luneburgovy čočky s gradientním indexem lomu v pásmu milimetrových vln využitelné jako antény nebo retro reflektory pro zlepšení širokoúhlového rozsahu pokrytí a stabilní efektivní odrazné plochy u pasivních bezčipových frekvenčně kódovaných radiofrekvenčně identifikovaných orientačních bodů, jenž mají velký potenciál pro využití sebe-lokalizace uvnitř budov.